Study of Resonant $B^0 \to X_{d/s}\,\ell^+\ell^-$ Branching Ratios

Aman Pavan Salikar

Master's Thesis
at the Faculty of Physics
Ludwig–Maximilians–Universität München
Chair of Elementary Particle Physics

Supervisor:
Prof. Dr. Thomas Kuhr

Munich, Septemeber 29, 2022

Die Untersuchung von Resonante $B^0 \to X_{d/s}\,\ell^+\ell^-$ Zerfallsverhältnisse

Aman Pavan Salikar

Masterarbeit
an der Fakulität für Physik
Ludwig–Maximilians–Universität München
Lehrstuhl für Experimentelle Flavorphysik

Betreuer:
Prof. Dr. Thomas Kuhr

München, den 29 September, 2022

Abstract

The thesis focuses on resonant processes of $B \to X\ell\ell$ decay using 1 ab^{-1} Monte-Carlo simulated data at Belle II. The channels being analysed are $B^0 \to K^0_s J/\psi, B^0 \to K^0_s \psi(2S), B^0 \to \pi^0 J/\psi, B^0 \to \pi^0 \psi(2S), B^0 \to K^*(K^+\pi^-)\gamma^*, B^0 \to \rho^0\gamma^*$. At the loop level, the cross section of the decay modes of $B^0 \to X_{d/s}\, \ell^+\ell^-$ is dependant on the matrix elements V_{cd} and V_{cs}. So this analysis concentrates on the ratio X_s to X_d which is essentially the ratio of the above two elements. This was found out to be 24.12290 ± 0.595297 for J/ψ resonance state and 23.90814 ± 2.87876 for the $\psi(2S)$ resonance state.

Contents

Chapter 1

Introduction

1.1 New Physics

The purpose of the Belle-II experiment is mainly to study b-quark physics. This in turn could give hints for New Physics (NP) that could give insight into the open questions of the Standard Model (SM), as well as make precision measurements of the CKM parameters. There are basically two different approaches to search for New Physics: a) Direct search : this involves search for new particles directly produced in the decays. The Large Hadron Collider (LHC) at Geneva focuses on the direct approach. b) Indirect search: With this approach, the existence of beyond the SM particles is revealed by measuring well-known rare decay processes, for which loop diagrams involving the yet undiscovered virtual particles could contribute to physically measurable observables, most importantly the branching ratio. This the approach taken by the Belle II collaboration. The advantage of using this approach is that this study is not limited by beam energy, meaning that the sensitivity to NP can be significantly higher for significantly lower beam energies and less background. The sensitivity of indirect NP searches at Belle II depends on the strength of the flavour violating couplings of the NP, thus resulting in the mass spectrum of the new particle/process effects between 1-100 TeV [11].

1.2 The Standard Model

The Standard Model is not the complete model to describe our universe and there is a constant thrive among particle physicists to search for New Physics. One of those concern measuring the CKM matrix elements to a high precision. Flavour Changing Neutral Currents, which are forbidden at the tree level in the Standard Model, are sensitive to the values of these elements.

The Standard Model, see Figure 1.1, is a theory which describes the strong, weak and electromagnetic interactions of elementary particles. Presently it is the best tested theory to describe these interactions as its prediction of the Higgs Boson has been verified independently by two experiments ATLAS and CMS at the Large Hadron Collider in

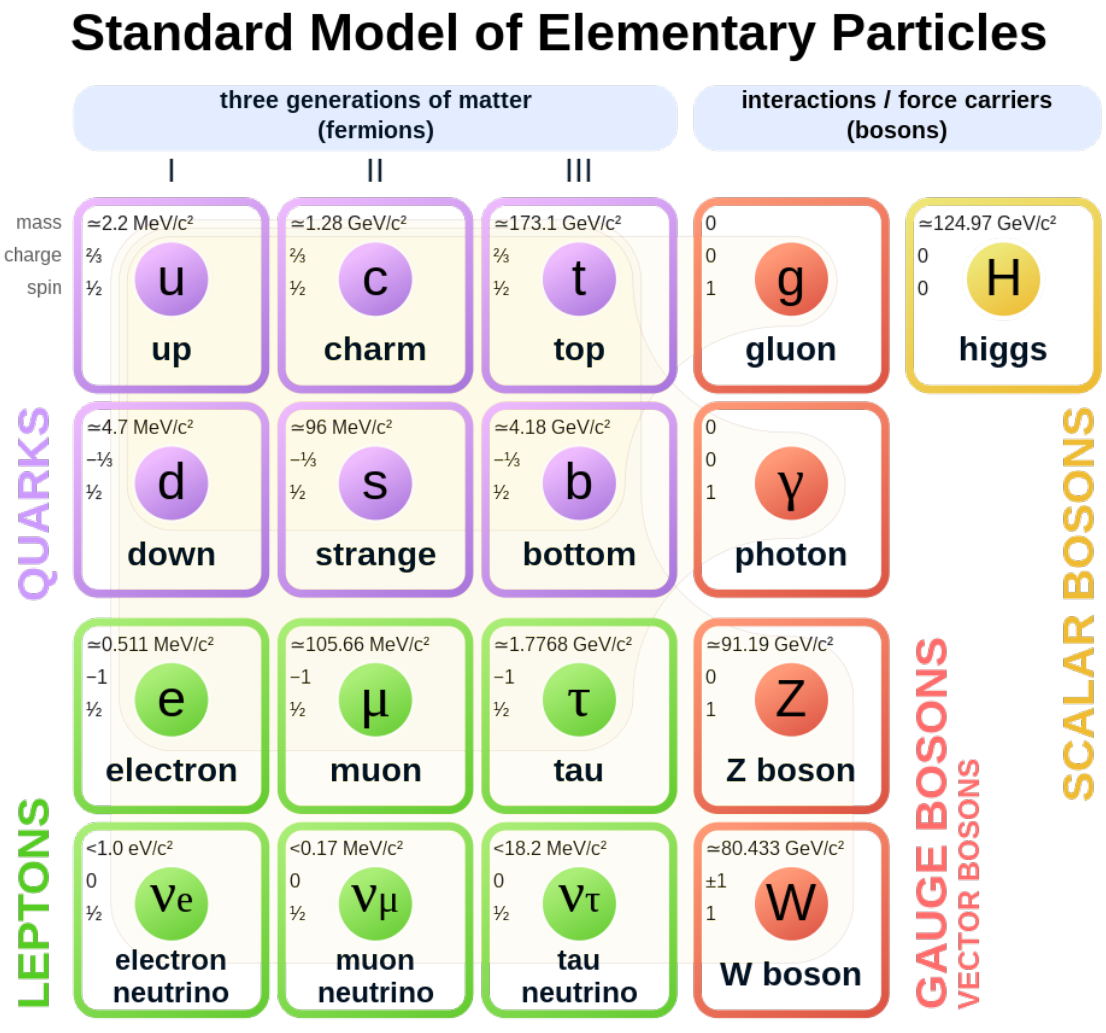

Figure 1.1: Elementary particles in the Standard Model [6]

2012. With this prediction, the unification of the electromagnetic and the weak force is also successfully predicted. In order to appreciate its beauty, a short review of the features of the particles and their interactions must be accounted for.

1.2.1 Fermions

Most of the matter which we see around us is mostly made up of just one generation of fermions, i.e. the up and the down quark (from the quark family) and electrons(from the lepton family) .The electron-neutrino, again from the lepton family, also belongs to this generation, however is mostly aloof to the real world phenomenon. All these are spin $\frac{1}{2}$ fermions. All the leptons can interact via the weak force. Besides the neutrinos, all the other species also interact with each other electromagnetically, however it is only the quarks which do interact strongly. Particles in the higher generations share the same quantum numbers as the ones in the lower generations, they only differ in their masses. However, this might not be the case for neutrinos as the mass hierarchy here is largely unknown.

1.2.2 Interactions

Fundamentally four kinds of interactions have been found to exist in nature. In the Standard Model however, gravitational force does not play a role. So let us look at the other three:

Electromagnetic interaction This interaction is described through the theory of quantum electrodynamics (QED), which is mediated by a vector boson named photon. As mentioned, neutrinos do not take part in these interactions.

Weak interaction This force is mainly responsible for radioactive decay processes such as ${}^{14}_{6}C \rightarrow {}^{14}_{7}N + e^- + \bar{\nu}_e$. The gauge bosons responsible for this interactions are heavy, in the sense that they are short-ranged.

Strong interaction This interaction is felt by the quarks only which helps them to produce bounded states of baryons and mesons. This interaction is mediated by 8 bosons called "gluons" which are massless.

1.2.3 Lagrangian

SM is based in the group $SU(3)_c \times SU(2)_L \times U(1)_Y$ which is spontaneously broken down to $SU(3)_c \times U(1)_{em}$ through the Higgs mechanism.

The fermions have a chiral spinorial representation $\psi_{L(R)} = \frac{(1+\gamma_5)}{2}\psi$, the gauge bosons have a vectorial representation. In the $SU(3)_c$ group, the quarks q_α have the fundamental representation and the rest of the fermions are singlets. In the $SU(2)_L$ group, the left handed fermions ψ_L are in the fundamental representation and the right handed fermions ψ_R are singlets. In the $U(1)_Y$ group, all the fermions are in the fundamental representation and they have charges according to the rule $Y = 2(Q - T_{3L})$, where Q is the electromagnetic charge and T_{3L} is the quantum number associated with the $SU(2)_L$ group. Along with this

we also have the scalar Higgs boson Φ. Before breaking the symmetry, we have the following Lagrangian:

$$\begin{aligned} L_{SM} = &-\frac{1}{4}\left(W_i^{\mu\nu}W^i_{\mu\nu} + G_a^{\mu\nu}G^a_{\mu\nu} + B^{\mu\nu}B_{\mu\nu}\right) + \frac{1}{2}\left(D^\mu\Phi\right)^\dagger\left(D_\mu\Phi\right) \\ &+ i\bar{\ell}_L\gamma^\mu D_\mu\ell_L + i\bar{q}_L^\alpha\gamma^\mu D_\mu q_{L\alpha} + i\bar{u}_R^\alpha\gamma^\mu D_\mu u_{R\alpha} + i\bar{d}_R^\alpha\gamma^\mu D_\mu d_{R\alpha} + i\bar{e}_R\gamma^\mu D_\mu e_R \\ &+ \left(y_d\bar{q}_L^\alpha\Phi d_{R\alpha} + y_u\bar{u}_L^\alpha\tilde{\Phi}u_{R\alpha} + y_e\bar{\ell}_L\Phi e_R + h.c.\right) - V\left(\Phi^\dagger\Phi\right) \end{aligned}$$

where $W^i_{\mu\nu} = \partial_{[\mu}W^i_{\nu]}$ and W^i_μ refers to the three W bosons of the $SU(2)_L$ group; $G^a_{\mu\nu} = \partial_{[\mu}G^a_{\nu]}$ and G^a_μ refers to the eight gluons of the $SU(3)_c$ group; $B_{\mu\nu} = \partial_{[\mu}B_{\nu]}$ and B_μ refers to the only single boson of the $U(1)_Y$ group; $D_\mu = \left(\partial - igW^i_\mu\frac{\sigma^i}{2} - ig'\frac{Y}{2}B_\mu\right)$.

By choosing the Φ to be $\begin{pmatrix}0\\v\end{pmatrix}$, we can break the $SU(2)_L \times U(1)_Y \to U(1)_{em}$ and as a result we get 3 massive gauge bosons and 1 massless gauge boson.

At the same time, mass terms for the fermions are also generated. The interactions of the fermions with the gauge fields itself does not mix families, as can be seen from the kinetic terms in the Lagrangian. However when we want to calculate some physical process, we always refer mass eigenstates, that is those which have a definite mass. In the Standard Model, which has more than one generation of leptons, the mass eigenstates are not the same as interaction eigenstates. Thus when we transform our basis to mass eigenstates basis, there will be family-changing interactions.

Let us specifically look at the neutral current term in the SM Lagrangian after symmetry breaking. It reads $L^0 = \bar{\psi}\gamma^\mu\left(\frac{g}{2}\sigma_3 W^3_\mu + \frac{g'}{2}YB_\mu\right)\psi$. Now defining $W^3_\mu = A_\mu sin\theta_W + Z_\mu cos\theta_W$ and $B_\mu = A_\mu cos\theta_W - Z_\mu sin\theta_W$ along with the definition of couplings $e \equiv gsin\theta_W = g'cos\theta_W$ we can rewrite the term as

$$L^0 = eA_\mu\bar{\psi}\gamma^\mu\left(\frac{\sigma_3}{2} + \frac{Y}{2}\right)\psi + \frac{g}{cos\theta_W}Z_\mu\bar{\psi}\gamma^\mu\left(T_{3L} - Qsin^2\theta_W\right)\psi$$

Here we notice that the first term is just the electromagnetic interaction. The second term shows the existence of another neutral interaction term, involving the Z boson, and this is felt by all fermions.

If we now write ψ as $\psi = \psi_L + \psi_R$ where $\psi_{L(R)} = \frac{1\pm\gamma_5}{2}$, we see that we can expand the above term as $L^0 = eA_\mu\bar{\psi}_L\gamma_\mu Q\psi_L + eZ_\mu\bar{\psi}_L\gamma_\mu\left(T_{3L} - Qsin^2\theta_W\right)\psi_L$ + right handed part. So now if we rotate the left(right)-handed field by a unitary matrix $U_{L(R)}$ (in order to go from flavour to mass basis), we see that in the end we get the same term as $U^\dagger_{L(R)}U_{L(R)} = 1$. So we see that the neutral currents do not mix families. However the weak currents play a very different role here. If we look at the term

$$L^\pm = \frac{g}{\sqrt{2}}W^+_\mu\bar{u}_L\gamma^\mu d_L + \bar{c}_L\gamma^\mu s_L = \frac{g}{\sqrt{2}}W^+_\mu\left(\bar{u}_L\bar{c}_L\right)\gamma^\mu\begin{pmatrix}d_L\\s_L\end{pmatrix}$$

Now if we try to rotate the fields as doublets individually, i.e.

$$\left(\bar{u}_L \bar{c}_L\right) \rightarrow U_{uL}^{\dagger} \left(\bar{u}_L \bar{c}_L\right) and \begin{pmatrix} d_L \\ s_L \end{pmatrix} \rightarrow U_{dL}^{\dagger} \begin{pmatrix} d_L \\ s_L \end{pmatrix}$$

we see that we get a non-vanishing term which we define as $V \equiv U_{uL}^{\dagger} U_{dL}^{\dagger}$ and we can write the interaction in the mass basis as

$$L^{\pm} = \frac{g}{\sqrt{2}} \left[\left(\bar{u}_L \bar{c}_L\right) \gamma^{\mu} V \begin{pmatrix} d_L \\ s_L \end{pmatrix} \right] W_{\mu}^{+}$$

For the leptons, we get similarly a doublet for the neutrinos and a doublet for the heavy leptons. But since the neutrinos are massless in the SM, we can safely rotate the neutrino doublet by any angle so as to cancel that with the rotation of the heavy leptonic doublet. So ultimately we see that lepton families do mix even in the charged sector.

For 3 generation of families, the matrix V is called V_{CKM}, where CKM stands for Cabibbo-Kobayashi-Maskawa. In the parameterized form it can be written as

$$V_{CKM} = \begin{pmatrix} c_{12}c_{13} & s_{12}c_{13} & s_{13}e^{-i\delta} \\ -s_{12}c_{23} - c_{12}s_{23}s_{13}e^{i\delta} & c_{12}c_{23} - s_{12}s_{23}s_{13}e^{i\delta} & s_{23}c_{13} \\ -s_{12}s_{23} - c_{12}c_{23}s_{13}e^{i\delta} & -c_{12}s_{23} - s_{12}c_{23}s_{13}e^{i\delta} & c_{23}s_{13} \end{pmatrix}$$

where $c_{ij} = cos\theta_{ij}$; $s_{ij} = sin\theta_{ij}$ and θ_{ij} are the three Euler angles.

1.3 Flavour Physics

So as we have seen, the neutral sector of the SM does not allow two fermions of different generations to interact with each other. In other words, this means that at the tree-level of interactions, the lepton flavour number is conserved. So for example the reaction $B^0 \rightarrow K_s^0 \phi$ would violate lepton flavour number as the b-quark transforms to s-quark. So at tree level, this interaction cannot involve the photon nor the Z boson. If however that were to be the case, such interactions, also known by the name Flavour Changing Neutral Current (FCNC) interactions would take place and this would constitute NP as this is not predicted by the SM. For this process to be allowed within the SM, one would need a loop-level interaction to achieve this. In general $B^0 \rightarrow X_{s/d} \ell^+ \ell^-$ processes belong the FCNC field. In fact, most of the FCNC sector is dedicated to B-physics. As we argued, we need loops to achieve this process. Now in these loops one can expect to find new particles , i.e. those predicted by theories beyond the SM, and thus affecting the branching ratio of reactions, angular distributions and other physical variables thus making this one of the areas of physics which could provide hints for NP. Now in the decay $B^0 \rightarrow X_{s/d} \ell^+ \ell^-$, the amount of X-species is not really known in great detail, in other words, the number of X-mesons with either a s-quark or a d-quark is not known. So instead of analysing the whole the spectrum of X-mesons which could take part in this process, in this analysis the focus has been on exclusively on the following states K_s^0, π^0, K^+ and ρ^0. For the leptons,

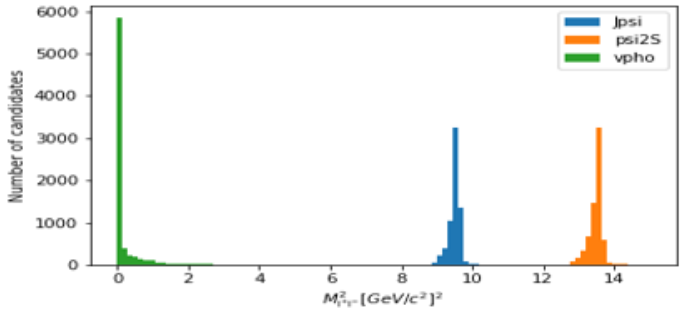

Figure 1.2: Distribution of di-leptonic mass-squared spectrum for signal events

1	$B^0 \to K^0_s J/\psi$
2	$B^0 \to K^0_s \psi(2S)$
3	$B^0 \to \pi^0 J/\psi$
4	$B^0 \to \pi^0 \psi(2S)$
5	$B^0 \to K^*(K^+\pi^-)\gamma^*$
6	$B^0 \to \rho^0 \gamma^*$

Table 1.1: Different decay channels to be analysed in this study

the $\ell^+\ell^-$ could actually be a $\mu^+\mu^-$ or a e^+e^- pair. This pair of leptons however is emitted from a leptonic resonance state. So similar to the mesonic part, only a select amount of leptonic resonant states have been considered, which are $J/\psi, \psi(2S)$ and γ^*, as can be seen in Fig 1.2.

From the Table 1.1, we see that we have ultimately 6 different channels, each with a cross section that depends on one or more CKM elements. In order to obtain the ratio X_s to X_d, the branching fraction of these 6 channels will be considered, which will in turn depend on the specific CKM elements as shown in Fig 1.3.

1.4 Belle II experiment

The Belle II experiment [7] (which comprises of the Belle II detector and the SuperKEKB accelerator) is a 3 km circumference asymmetric electron–positron collider which specializes in high-precision measurements of rare decays and CP-violation in heavy quarks and leptons, thus providing a unique probe of New Physics. The aim of the experiment is to accumulate an integrated luminosity of 50 ab^{-1} by 2035 [8].

The SuperKEKB 1.4 operates mostly at the energy of the $\Upsilon(4S)$ resonance which around 10.58 GeV. This ensures that the corresponding B meson pairs produced are essentially at rest in the center of mass reference frame.

The Belle II detector 1.5 is, simply put, a huge magnetic spectrometer which surrounds

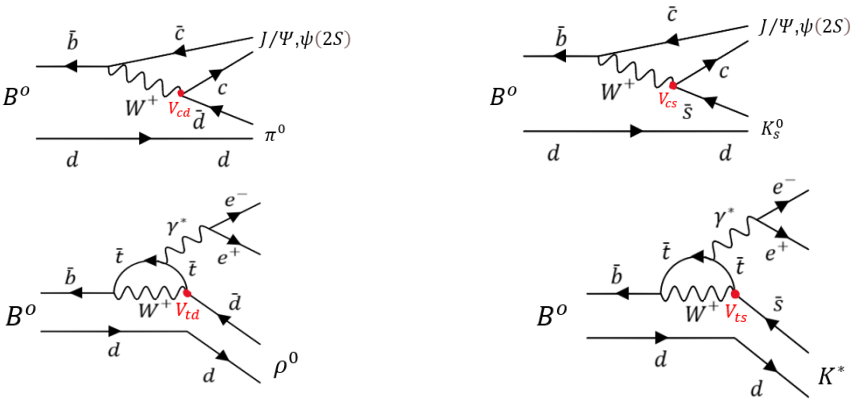

Figure 1.3: Feynman diagrams for various processes

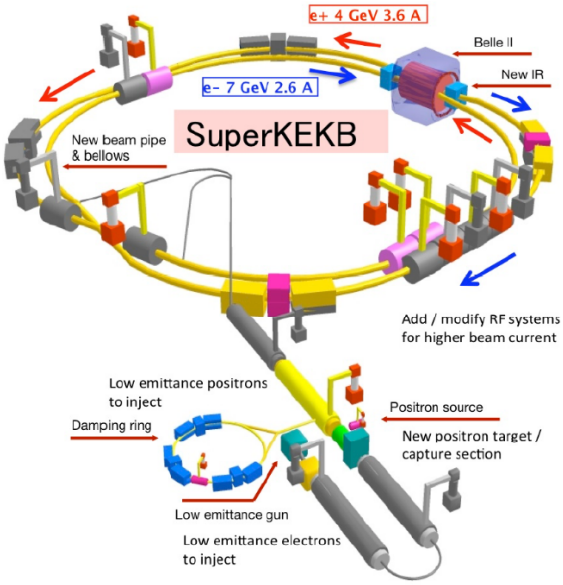

Figure 1.4: Schematic view of the SuperKEKB factory

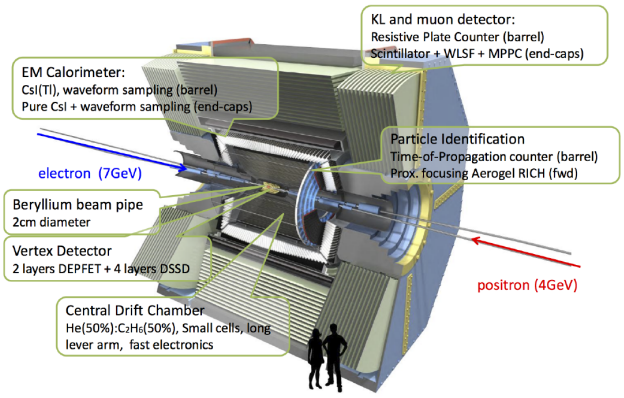

Figure 1.5: Schematic view of the Belle II detector [2]

the SuperKEKB interaction point. The detector itself comprises of many different sub-level detectors:

1.4.1 Vertex detector (VXD)

It is the innermost detector surrounding the beam pipe region [12]. It is divided into two parts- the Silicon Pixel Detector (PXD), which consists of pixelated sensors based on the DEPFET (DEPleted Field Effect Transistor) technology, located between 14 mm and 22 mm from the interaction point. This technology allows for very thin pixel sensors which have a large number of channels and small occupancy, making them suitable to cope with increased event rates. The remaining four layer around the PXD correspond to the Silicon Vertex Detector (SVD). They comprise of double-sided silicon strip sensors distributed between radii of 38 mm and 140 mm. Thanks to the DEPFET sensors closer to the interaction point and the more distant silicon strips, Belle II benefits from an improved vertex resolution.

1.4.2 Central Drift Chamber (CDC)

This is simply put a tracking system surrounding the VXD [12]. It comprises of a cylindrical chamber filled with a mixture 50% helium and 50% ethane. The inner chamber structure comprises of 56 layers of wires, distributed into 9 super-layers, which can be axial ("A") or stereo ("U" or "V"), depending on the wire configuration. Stereo super-layers are disposed such that they form a non-zero angle with the z-axis, which was determined in order to maximize z-measurement capabilities and z-trigger performance.The CDC is in charge of reconstructing charged tracks and from that one can measure the momenta. Also, it provides particle identification information by measuring the energy lost in the gas volume. Along with this it provides trigger signals for charged tracks.

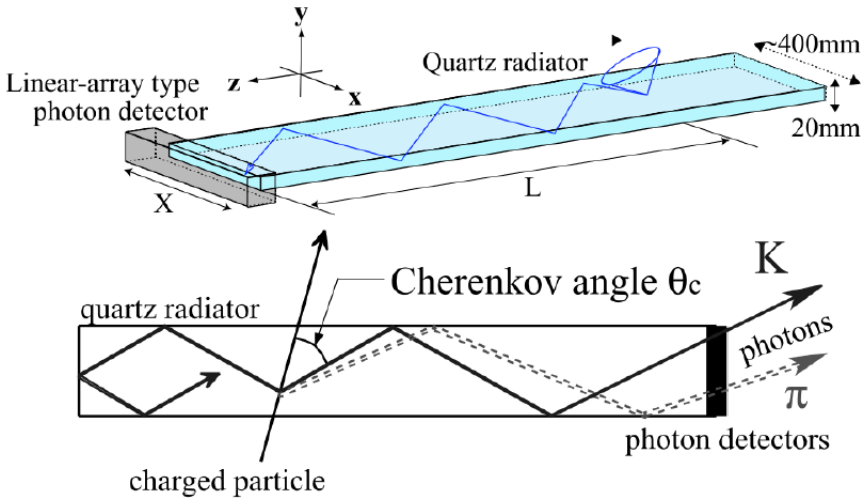

Figure 1.6: Schematic top and side view of the TOP counter

1.4.3 Time-of-Propagation (TOP) Detector

The TOP 1.6 is a Cherenkov counter located in the barrel region of the Belle II detector [12]. Together with the ARICH sub-detector, these two are dedicated particle identification systems. The 16 detection modules of the TOP counter comprise of quartz bars 260 cm long, 45 cm wide and 2 cm thick surrounding the outer wall of the CDC. The TOP counter works by measuring some of the Cherenkov photons emitted by a charged particle travelling through the quartz radiators faster than the speed of light in the material. These photons are then internally reflected by the walls of the radiator until they collide with the photon detector, as shown at the bottom in Figure .

The position in the (x, y) plane and the time of detection of the photon are measured this way and used to reconstruct a Cherenkov image. The distribution of times of arrival for the photons is then compared with the known probability density functions (PDFs) of all particle hypothesis1, which then provides the identification information.

1.4.4 Aerogel Ring Image CHerenkov (ARICH) Detector

The ARICH 1.7 is also part of the particle identification system and is located in the forward end cap of the detector [12]. This counter is designed to separate kaons and pions up to momenta of about 4 GeV/c, as well as separate electrons muons and pions for studies of rare b-quark decays. Similar to the TOP, the ARICH is also a Cherenkov detector which consists of a radiator and a photon detector system. In the case of this sub-detector, the radiator body is made up of two 2 cm thick layers of silica aerogel. These two silica tiles are positioned consecutively and have different refractive indices. Specifically, the tile on upstream side has a refractive index n = 1.046, while for the one on the downstream side

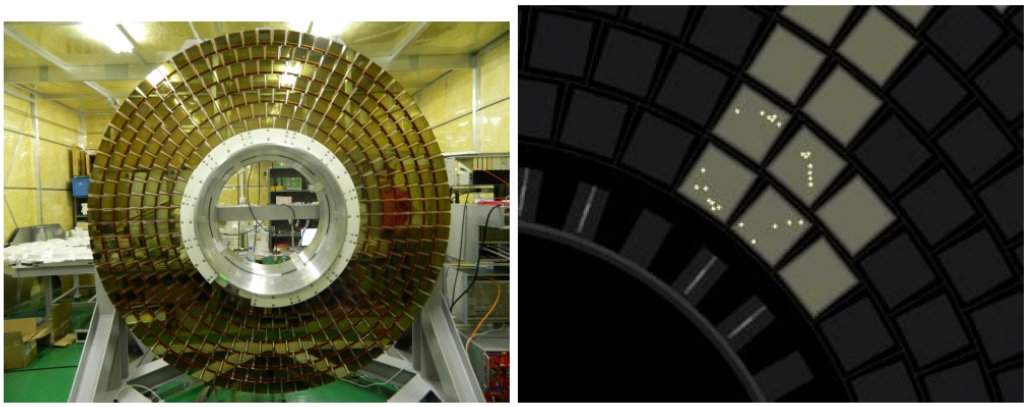

Figure 1.7: (Left) Photo of the ARICH detector. (Right) Event display of a ring produced by a cosmic muon [12]

n = 1.056. This design choice allows for a much higher performance, compared to a single thicker layer of aerogel silica.

1.4.5 Electromagnetic Calorimeter (ECL)

The ECL is used to measure photons by precisely determine their energy and angular coordinates, as well as identifying charged particles. Through the energy deposited by the particles when passing through the ECL, it also offers limited Particle Identification (PID) capabilities. The calorimeter used in Belle II is very similar to the one used in Belle [12]. The only differences come from the upgraded electronics and the replacement of the scintillator crystals at the endcap. The detector consists of a barrel and two endcaps regions filled with 8736 crystal scintillators. The 3 m long barrel region contains 6624 thallium-doped caesium iodide CsI(Tl) crystals assembled in a projective geometry, while the endcaps contain the remaining 2112 CsI crystal arrays. The inner radius of the barrel measures 1.25 m, and the forward and backward annular endcaps are located 1.96 m and -1.02 m from the IP respectively.

1.4.6 Long-kaon and Muon Detector (KLM)

This is the outermost sub-detector [12]. As the name suggests, it is used to detect the muons and long kaons from the decay process. The body of the kaon long - muon detector consists of an octagonal barrel surrounding the Belle II 1.5 T superconducting solenoid magnet, completed by two endcaps in the forward and backward regions of the detector. The KLM is filled with a total of 43 detector elements consisting of glass electrode resistive-plate-chambers (RPC), of which 15 are located in the barrel region and 14 in each endcap. In between each plate lies a a 4.7 cm thick iron plate, leading to a sandwich-like configuration of detector elements and iron plates. The iron serves as the magnetic flux return for the

solenoid, as well as providing 3.9 interaction lengths or more of material in which the K_L can shower hadronically. The RPC consist of two sheets of glass with a noryl spacer in between, filled with a gas mixture of 62% HFC-134a, 30% argon, and 8% butane-silver. A charged particle is detected via its ionizing effect when it passes through the gas. The KLM is designed to detect muons and long lived neutral kaons, especially to distinguish them from pions. The design allows for good separation of muons from pions at momenta above 1 GeV/c and good kaon-pion separation above 3 GeV/c.

Chapter 2

Main Analysis Procedure

The analysis of $B^0 \to X_{s/d}\ell^+\ell^-$ relies on the Belle II software. The Belle II datasets used for this analysis contain fully reconstructed events.

2.1 Software and Datasets

For this analysis, the following softwares were used:

1) BASF2 (version 06-00-03) : Belle II Analysis Software Framework [13] is the essential software foundation for Belle II data analysis.

2) GBASF2 (version v5r5) : Grid-BASF2 [3] is the distributed-computing structure of Belle II collaboration consisting of numerous sites around the world for storing data locally and responsible for running large Monte-Carlo (MC) campaigns.

3) zFit [9] (version 0.8.3) : Fitting software used to estimate the number of signal events by fitting the data to certain probabilistic distributions.

4) Snakemake [5] and b2luigi [1] are both workflow programs which offer a great advantage to the analyst as it makes the process repeatable for different inputs and thus helping the whole framework become more analyst-friendly.

Along with this, the following datasets were used for analysis:

1) Signal Monte-Carlo analysis: MC-15 based data for 25,000 events for each individual decay mode.

2) Generic Monte-Carlo analysis: MC-15b run-independent dataset corresponding to 1 ab^{-1} of data.

2.2 Signal Monte-Carlo analysis

2.3 Analysis flow

1. Final particles found in the sample are first to the added to our analysis object. At the same time, cuts are made to these lists so as to select only those particles which would be

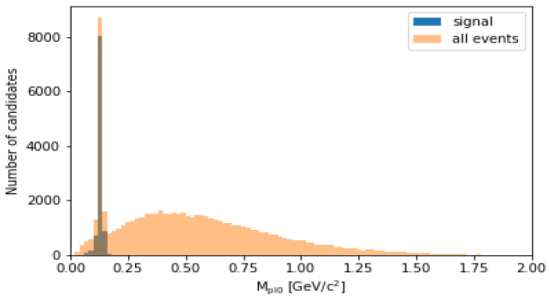

Figure 2.1: Pion mass distribution before any selection cuts

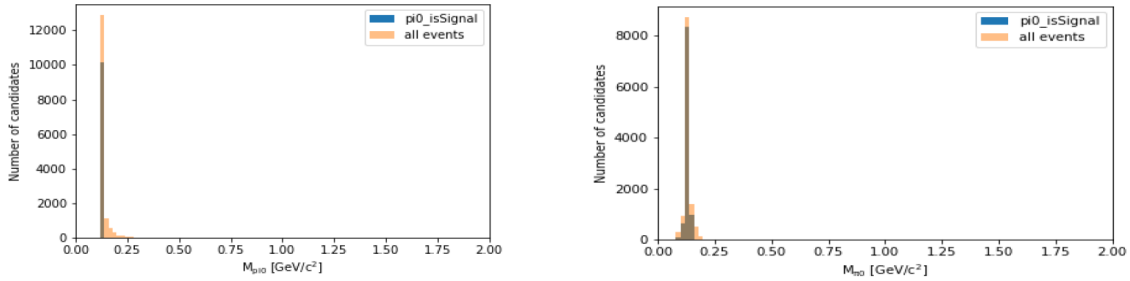

Figure 2.2: (Left) Pion mass distribution after a mass fit. (Right) Pion mass distribution after a selection cut

useful for the analysis. Following are the cuts made on the final lists

"**good**" selection criteria (for electrons, positrons, muons, charged pions and charged kaons), which includes the following:

- To check if the particle polar angle is within the CDC acceptance;
- Number of CDC hits associated to the track > 20;
- Transverse distance with respect to Interaction Point for a vertex < 0.5 cm;
- Point of closest approach along z-axis with respect to IP < 2 cm;
- PID (Particle Identification information variable) > 0.5 .

For the neutral pions, the list had to pass a selection criteria before it could be used for the analysis, as can be seen from Fig 2.1 due to immense amount of background pions. Two known methods could be used overcome this problem:

a) Use a pre-defined mass fit on the list to selectively pick out those pions which are signal events. However, this also results in a certain amount of redistribution of pion mass distribtuion events;

b) Use a cut of $|\ \delta M\ | < 0.05$ GeV/c^2 on the list to selectively narrow out the distribution and hence select mostly signal events, see 2.2 .

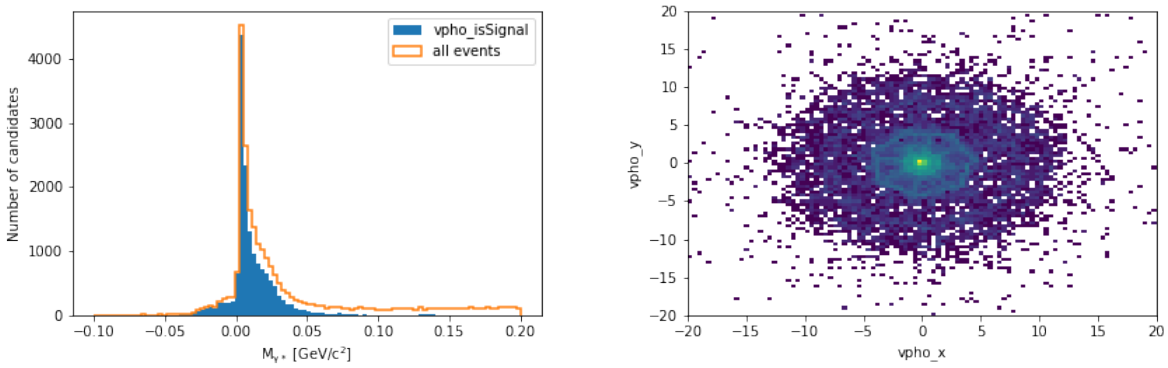

Figure 2.3: (Left) Virtual photon mass distribution, with a cut M $<$ 0.2 GeV/c^2. (Right) Virtual photon decay vertex distribution. As can be seen, the various components of the detector also become highlighted through this plot.

For K_s mesons a simple vertex fit is performed, along with which a certain cut on the invariant mass in the range 0.450<M<0.550 GeV/c^2 is implemented.

This ensure that we have high purity lists for data studies.

2. From these final particle lists, one can recombine to form intermediate particles (again implementing cuts in order to reduce background events).

An interesting case arises for the virtual photons, as can be seen in Fig 2.3. Some of the events also show in the negative mass region, however this does not provide a problem for the analysis as finally for the reconstruction of mother B^0 meson it does not play that significant a role.

3. From the intermediate particle lists one can then reconstruct the mother B^0-meson, with a cut on the beam-constrained mass.

4. Vertex fitting algorithms are also implemented in order to select the required mother particles on the basis of their decay vertices.

5. Bremsstrahlung correction is added as shown in Fig 2.4.

6. Along with this information, for MC-matching, the isSignal variable is also added.

7. For better analysis results, tag-side information is also added.

8. Continuum event information like R2 (see appendix) is also added to in order to reduce continuum background.

9. All of this information is then saved to an n-tuple file.

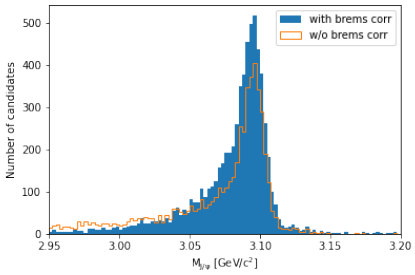

Figure 2.4: J/ψ mass distribution before and after introducing the Bremsstrahlung correction. As can be seen in the figure, the left part of the earlier distribution gets shifted towards the centre indicating that electrons responsible for these events are compensated for their energy loss due to Bremsstrahlung radiation.

Decay	Efficiency	Purity		Decay	Efficiency	Purity
$B^0 \to K_s^0 J/\psi(e^+e^-)$	0.3063	0.8437		$B^0 \to K_s^0 J/\psi(\mu^+\mu^-)$	0.4951	0.8341
$B^0 \to K_s^0 \psi(2S)(e^+e^-)$	0.3356	0.8712		$B^0 \to K_s^0 \psi(2S)(\mu^+\mu^-)$	0.5202	0.8575
$B^0 \to \pi^0 J/\psi(e^+e^-)$	0.2993	0.7472		$B^0 \to \pi^0 J/\psi(\mu^+\mu^-)$	0.4974	0.7433
$B^0 \to \pi^0 \psi(2S)(e^+e^-)$	0.3146	0.7705		$B^0 \to \pi^0 \psi(2S)(\mu^+\mu^-)$	0.5273	0.7621

Table 2.1: Tables for (left) electron decay modes and (right) muon decay modes

After obtaining the resulting n-tuple file, a study was conducted to investigate the resulting efficiencies from two different decay modes of the B^0 meson, one through electrons and one through muons. To do this, one defines the efficiency and purity of the analysed dataset as follows:

$$\text{Efficiency} = \frac{\text{Number of truth-matched candidates}}{\text{Number of generated events}}$$

$$\text{Purity} = \frac{\text{Number of truth-matched candidates}}{\text{Total number of reconstructed candidates}}$$

In Table 2.1 the result of this study is presented. As can be seen, the muons modes have substantially more efficiency and more or less the same purity. This is a result of the higher PID associated with muons compared to electrons as it is well known that reconstructing muons is far more efficient than reconstructing electrons.

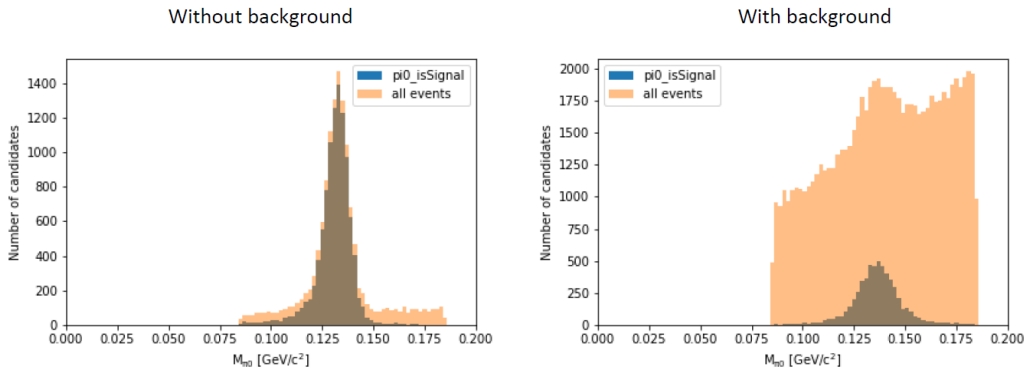

Figure 2.5: (Left) Pion mass distribution for signal MC dataset. (Right) Pion mass distribution for generic MC dataset

2.4 Generic Monte-Carlo analysis

When the analysis was carried over the generic MC dataset, the amount of background to be investigated also substantially increase, as can be seen from the pions in Fig 2.5. The main reason for this background was found out to be coming from the energies of daughter photons, as can be seen in the four plots in Fig 2.6

To find the optimum cut, a certain variable defined as Figure of Merit (FoM) is defined through

$$\text{FoM} = \frac{\text{Number of Signal Events}}{\sqrt{\text{Number of Signal Events}} + \sqrt{\text{Number of Background Events}}}$$

through which we get the optimum cut for the daughter photons energy to be 0.13GeV.

Similar to this, another major background source were the continuum event states, that is those which do not come from the resonant $\Upsilon(4S)$ meson decay, but certain other resonant states like $\Upsilon(1S)$ or $\Upsilon(2S)$ and others which have pretty much the same decay products. To distinguish those from our designated decay channels, certain continuum suppression variables like R2, which is defined as ratio of the i-th to the 0-th order Fox Wolfram moments of the decay products, are used to distinguish between signal and background events. One such case is shown in Fig 2.7.

After making such cuts on the remaining channels, the following distributions of the M_{bc} (beam constrained mass) variable were obtained for the different channels, see Fig 2.8.

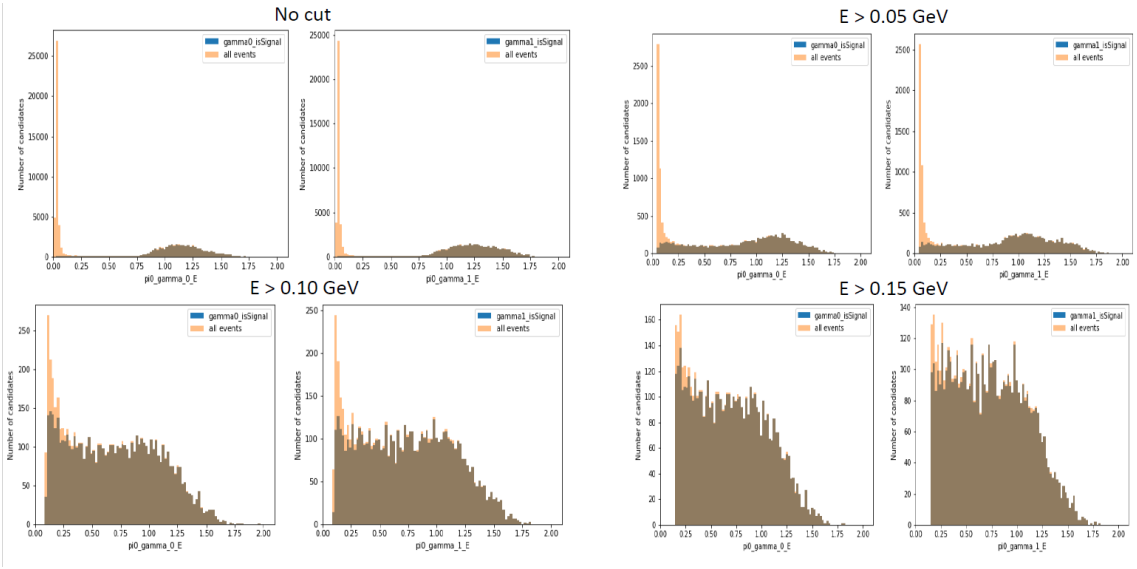

Figure 2.6: Different pion's daughter photon mass distributions for different cuts on their respective energies, for both the daughters simultaneously.

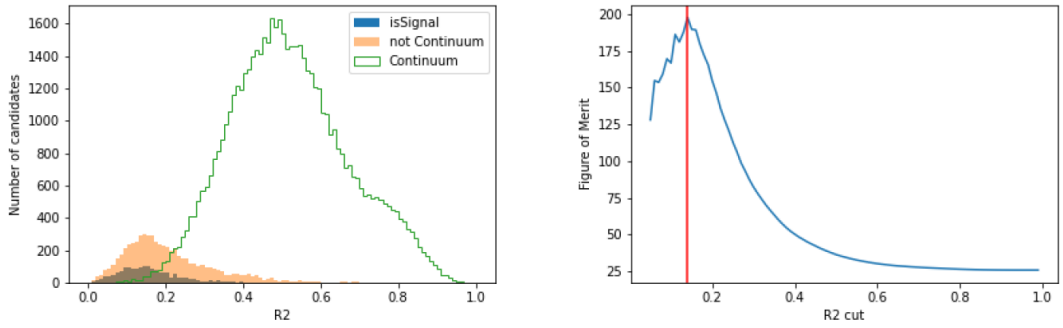

Figure 2.7: (Left) R2 distribution for $B^0 \to K^0_s J/\psi$ channel. (Right) FoM plot for R2 to select the optimum cut value at 0.17.

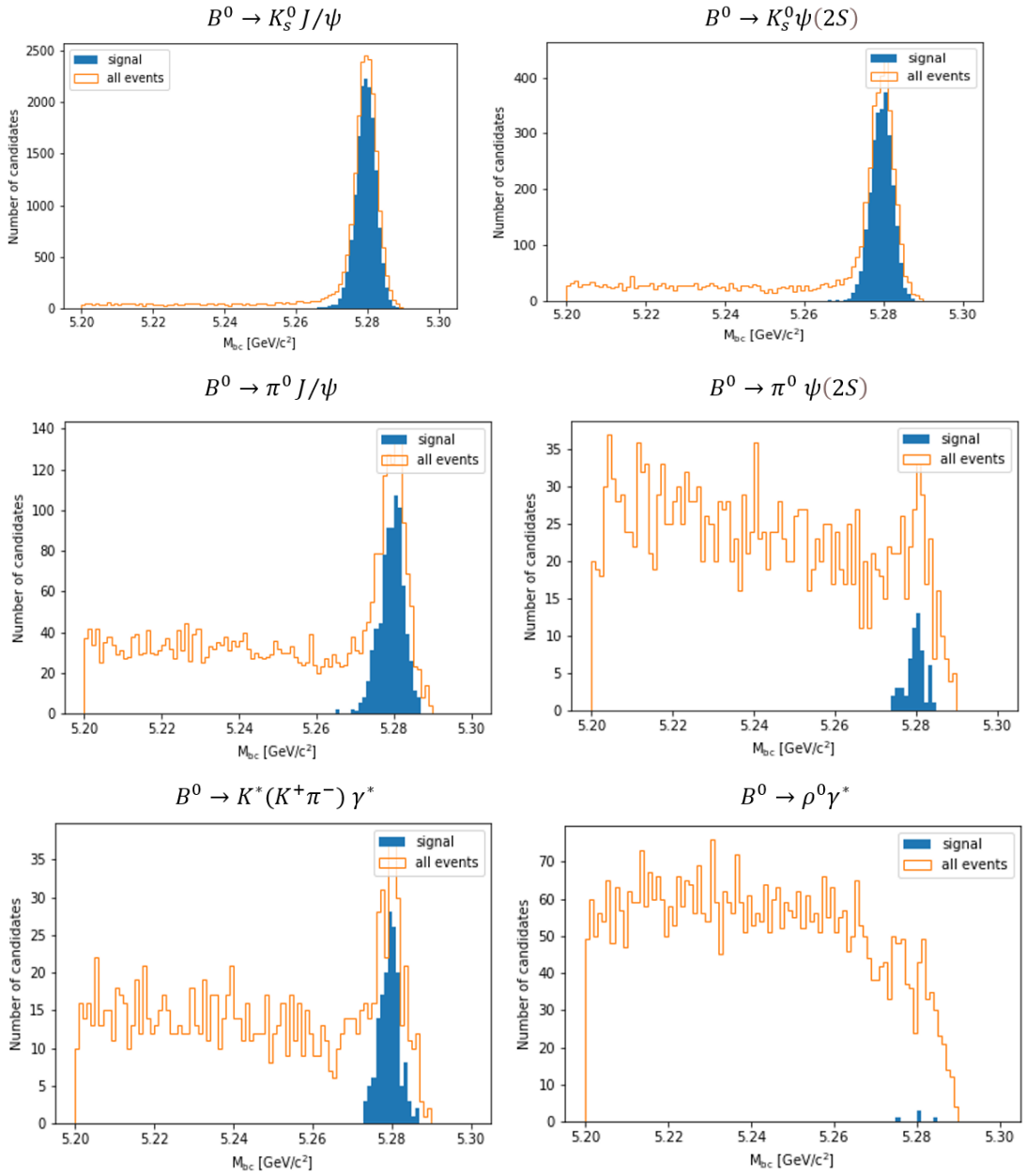

Figure 2.8: Different M_{bc} distributions for different decay channels.

		Extracted signal events	Truth-matched signal events
1	$B^0 \to K^0_s J/\psi$	15,393.498 ± 95.964	15440
2	$B^0 \to K^0_s \psi(2S)$	2,489.175 ± 45.4434	2506
3	$B^0 \to \pi^0 J/\psi$	745.0128 ± 32.9094	752
4	$B^0 \to \pi^0 \psi(2S)$	56.94782 ± 7.64589	55
5	$B^0 \to K^*(K^+\pi^-)\gamma^*$	155.7976 ± 15.528	150
6	$B^0 \to \rho^0 \gamma^*$	6.881338 ± 21.051	5

Table 2.2: Table for final fit values

2.5 Fitting

Following a careful study of the distribution of various variables and after improvising the cuts, another analysis is made to run over the grid in order to obtain best possible n-tuple file. With this file, the fitting procedure is implemented. In this analysis, the M_{bc} variable is used to extract the number of signal events. The fit results are presented in Table 2.2

Chapter 3

Results of the Analysis

Using the formula for the Branching Ratio (BR) for a general B^0 meson decay [10]

$$BR(B^0 \to X\ell\ell_{res}) = \frac{N_{B^0 \to X\ell\ell_{res}}}{2 \times N_{B^0B^0} \times \epsilon_{sig} \times BR(X \to \pi^+\pi^-/\gamma^0\gamma^0/K^+\pi^-) \times BR(\ell\ell_{res} \to e^+e^-/\mu^+\mu^-)}$$

where, $N_{B^0 \to X\ell\ell_{res}}$ refers to the number of extracted signal events
$N_{B^0B^0}$ refers to the number of B^0 pairs.
ϵ_{sig} refers to the signal efficiency
and BR( ) refers to the respective branching ratio.

and applying it to all but one of the decay channels, we get the following values for the branching ratio as shown in Table 3.1.

The fit result for $B^0 \to \rho^0\gamma^*$ does not produce a reliable number of signal events, in the sense, the uncertainity in the extracted number of signal events is much too large when compare to the actual number of signal events. Thus this makes the channel unfit for further studies and more statistics are required in order to infer better results.

		Reconstructed BR	PDG value [14]
1	$B^0 \to K^0_s J/\psi$	$(4.3275431 \pm 0.008657) \times 10^{-4}$	$(4.37 \pm 0.32) \times 10^{-4}$
2	$B^0 \to K^0_s \psi(2S)$	$(3.1598412 \pm 0.02487) \times 10^{-4}$	$(3.1 \pm 0.5) \times 10^{-4}$
3	$B^0 \to \pi^0 J/\psi$	$(1.7939547 \pm 0.044125) \times 10^{-5}$	$(1.76 \pm 0.16) \times 10^{-5}$
4	$B^0 \to \pi^0 \psi(2S)$	$(1.321659 \pm 0.15880) \times 10^{-5}$	$(1.17 \pm 0.19) \times 10^{-5}$
5	$B^0 \to K^*(K^+\pi^-)\gamma^*$	$(2.73941458 \pm 0.113746) \times 10^{-6}$	-

Table 3.1: Table for final BR values

To measure the final ratio of X_s to X_d, the ratio of the reconstructed BR for $B^0 \to K_s^0 J/\psi$ v/s $B^0 \to \pi^0 J/\psi$ is taken and similarly for $B^0 \to K_s^0 \psi(2S)$ v/s $B^0 \to \pi^0 \psi(2S)$ (the statistical uncertainity is calculated according to [4]). The value for the J/ψ resonance is **24.12290 ± 0.595297** and that for the $\psi(2S)$ resonance is **23.90814 ± 2.87876** .

Chapter 4

Ideas for Analysis continuation

- A study concerning systematic uncertainties must be carried out to ascertain a better reconstructed BR value.
- Analysis of real data also must be taken into account in order to further improve the analysis flow as such.
- A fully inclusive analysis of $B^0 \to X_{s/d}\ell^+\ell^-$ can be carried out to finally compute the true ratio of X_s to X_d.

Summary

In this thesis, we have exclusively studied various different decay channels of the form $B^0 \to X_{s/d}\ell^+\ell^-$, thereby laying a focus on the effective computation of the CKM elements through the ratio of X_s to X_d mesons. The 6 decay channels mentioned in this study act as control channels for the fully inclusive analysis of $B^0 \to X_{s/d}\ell^+\ell^-$. This was done by taking 1 ab^{-1} of generic Monte-Carlo simulated Belle II data as analysis object, from which signal events were extracted and the Branching Ratio was reconstructed. This was then used to construct the final ratio of X_s to X_d for two leptonic resonant states J/ψ and $\psi(2S)$. The values were found out to be 24.12290 ± 0.595297 for J/ψ resonance state and 23.90814 ± 2.87876 for the $\psi(2S)$ resonance state.

List of Figures

List of Tables

Appendix A

Signal MC Analysis

Since for the analysis recent signal-MC files were not found in the repository, they had to be generated. For each decay channel 25,000 events were generated. There are several steps that are involved in the Snakemake [5] workflow: 1. Generation of events using EventGen [12] . This relies mostly on the differential cross section of the process and generates final state particles. 2. Simulation of events using GEANT4 [12]. This step receives the final state particles, creates the hits in the detectors which in turn provides the simulation for the whole decay (also included is beam background simulation). 3. Reconstruction of events. The step reconstructs the final decay using the tracks from the ECL and KLM clusters and helps in identifying the particles.

The steps 1 and 2 are specifically executed for MC data, but the step 3 is common to both real and MC data. These events are then stored in a ROOT file which would be then the sample for the main analysis script, also called steering file.

Appendix B

Generic MC Analysis

For the analysis on the grid, i.e. for the generic Monte-Carlo files, b2luigi [1] workflow software was used. For this to be used, first the LFNs of the required MC files was needed to be saved in a file. After saving this file, the following steps are executed:

1. To ascertain if the analysis does run successfully, a few number of scout jobs are first submitted to the grid, i.e. at certain sites in the grid network which locally possess the data to be analysed, the jobs are submitted at random to these sites to be locally analysed.

2. After the scout jobs are successfully analysed, the remaining required jobs are submitted to various grid sites.

3. After successful completion of all the jobs, the output of these jobs is downloaded individually from their respective site.

4. After downloading, the outputs are then merged and we have the final n-tuple ready for analysis.

Bibliography

[1] b2luigi. https://b2luigi.readthedocs.io/en/stable/.

[2] Belle II detector. https://www.phy.olemiss.edu/HEP/belle2/index.html.

[3] GBASF2. https://software.belle2.org/sphinx/release-05-02-17/online_book/computing/gbasf2.html.

[4] Propagation of uncertainty. https://en.wikipedia.org/wiki/Propagation_of_uncertainty.

[5] Snakemake. https://github.com/snakemake/snakemake.

[6] Standard Model Diagram. https://en.wikipedia.org/wiki/File:Standard_Model_of_Elementary_Particles.svg.

[7] Super KEKB and Belle II. https://www.belle2.org/project/super_kekb_and_belle_ii.

[8] SuperKEKB Luminosity Projection. https://www-superkekb.kek.jp/Luminosity_projection.html.

[9] zfit. https://zfit.readthedocs.io/en/latest/index.html.

[10] A. Abdesselam et al. Measurement of the inclusive $B \to X_{s+d}\gamma$ branching fraction, photon energy spectrum and HQE parameters. In *38th International Conference on High Energy Physics*, 8 2016. https://inspirehep.net/literature?sort=mostrecent&size=25&page=1&q=find%20eprint%201608.02344.

[11] Abe, T. and others. Belle II Technical Design Report. *1011.0352*, 11 2010. https://inspirehep.net/literature?sort=mostrecent&size=25&page=1&q=find%20eprint%201011.0352.

[12] W. Altmannshofer et al. The Belle II Physics Book. *PTEP*, 2019(12):123C01, 2019. [https://inspirehep.net/literature?sort=mostrecent&size=25&page=1&q=find%20eprint%201808.10567].

[13] T. Kuhr, C. Pulvermacher, M. Ritter, T. Hauth, and N. Braun. The Belle II Core Software. *Comput. Softw. Big Sci.*, 3(1):1, 2019. `https://inspirehep.net/literature?sort=mostrecent&size=25&page=1&q=find%20eprint%201809.04299`.

[14] R. L. Workman and Others. Review of Particle Physics. *PTEP*, 2022:083C01, 2022. `https://pdg.lbl.gov/2022/tables/contents_tables.html`.

Acknowledgements

I would like to Prof. Dr. Thomas Kuhr from the bottom of my heart for allowing me to be part of his research group and for being very accommodating and understanding for all my wishes until the very end. I am also grateful to Dr. Sviatoslav Bilokin for his uncountable patience towards my slacky work-attitude and very kindly aiding me through the whole duration of my Master Project term. The whole credit really goes to him for making my work possible. Finally I want to thank all the other group members of the working group for their invaluable suggestions and critic via useful discussions at the weekly group meetings. It certainly pays off after being nagged for every tiny detail that might be easily overlooked by a single individual, thus making the work more robust and detailed.

Erklärung/Declaration

Hiermit erkläre ich, die vorliegende Arbeit selbständig verfasst zu haben und keine anderen als die in der Arbeit angegebenen Quellen und Hilfsmittel benutzt zu haben.

I hereby declare that this thesis is my own work, and that I have not used any sources and aids other than those stated in the thesis.

München, 29.09.2022
Aman Pavan Salikar